Fibrillation Behavior of Oriented Tapes of Polyethylene and Its Blends. IV

S. J. MAHAJAN,[1] B. L. DEOPURA,[1,*] and YIMIN WANG[2]

[1]Textile Technology Department, Indian Institute of Technology, New Delhi 110016, India, and
[2]Chemical Fibre Research Institute, China Technical University, Shanghai 200051, China

SYNOPSIS

This article reports a critical appraisal of the factors affecting fibrillation behavior (axial splitting tendency) of uniaxially oriented tapes prepared from high-density polyethylene and its blends. The drawn tapes were characterized by combined tension–twist fibrillation test, a new test proposed for this work. In addition, the drawn tapes were also characterized for microstructural details such as amorphous phase orientation, degree of crystallinity, void characteristics, and fracture surface morphology. It was found that an increase in amorphous phase orientation and degree of crystallinity systematically decreases the fibrillation strength and fibrillation toughness of tapes. General structural models to explain this phenomenon via microcrack formation, interfibrillar shearing process, and failure are proposed. © 1996 John Wiley & Sons, Inc.

INTRODUCTION

It is now well established that structure of uniaxially oriented fibers and tapes is of fibrillar character with extremely anisotropic morphology and mechanical properties. The fibrillar structure of these materials mainly consists of fibrils oriented in drawing direction and held together laterally, primarily by much weaker cohesive forces.[1-5] The structure has a high elastic modulus and tensile strength in the axial direction and tends to fibrillate under the influence of lateral tensile forces and very often under the influence of torsional, bending, or longitudinal shear forces.[6-22]

The fibrillation behavior of textile fibers has been extensively studied by many research workers.[6-22] However, only few studies[23-31] have involved the fibrillation behavior of thin, oriented tapes of rectangular cross-section, owing to the nonavailability of proper testing procedures. Recently, the use of polyolefin tapes in industrial applications such as woven sacks, fibrillated tape yarns, ropes, geotextiles, has increased the need to tailor the tape properties according to end-use requirements; interest is steadily developing in understanding the effects of structure–morphology on fibrillation behavior of tapes. For example, a easily fibrillating tape is a necessary prerequisite for production of fibrillated tape yarns, but it is undesirable in applications such as woven sacks where the fibrillation of tape seriously affects the production rates and quality of woven sack fabric. The fibrillation of tape, in this case, occurs as a result of abrasion and repeated axial, torsional, and bending forces generated during fabric manufacturing processes.

The present work is a preliminary study in this direction and gives information on interrelationships between some of the structural and morphological aspects of oriented polyethylene tapes and associated fibrillation behaviour.

EXPERIMENTAL

Materials

High-density polyethylene (HDPE), polypropylene (PP), high-molecular-weight high-density polyethylene (HMWPE), linear low-density polyethylene (LLDPE), low-density polyethylene (LDPE), ethylene vinylacetate (EVA), ethylene-propylene-diene

* To whom the correspondence should be addressed.

Journal of Applied Polymer Science, Vol. 60, 1551–1560 (1996)
 CCC 0021-8995/96/101551-10

Table I Characteristics of Materials Used

Polymer Type	Commercial Code	Supplier	MFI*	Density (g/cm^3)	Comonomer Type and Composition
HDPE	GF 7745F	PIL, India	0.7	0.945	1.8 CH_3/100 C
HMWPE	GF 7755	PIL, India	0.4	0.953	2.1 CH_3/100 C
LLDPE	Dowlex-2045E	Dow Chem. Co., U.S.A.	1.0	0.920	3.2 CH_3/100 C (L-octene)
LDPE	Dowlex-200	Dow Chem. Co., U.S.A.	0.9	0.920	3.6 CH_3/100 C
EVA	Elvax-4210	DuPont, USA	0.8	0.928	4.7 mol % vinylacetate
EPDM	Nordel-1040	DuPont, USA	40†	0.560	75 mol % ethylene and 4 mol % diene
PP	S-3030	IPCL, India	3.0	0.910	Isotactic homopolymer
EP_bC 1.5	MI-1530	IPCL, India	1.5	0.900	6.9 mol % ethylene
EP_bC 3.5	MI-3530	IPCL, India	3.5	0.900	6.8 mol % ethylene
EP_bC 7.0	MI-7040	IPCL, India	7.0	0.900	7.2 mol % ethylene
EP_bC 13.0	MI-0030	IPCL, India	13.0	0.900	6.6 mol % ethylene

* ASTM D1238/L.
† Moony viscosity 40, measured at ML4 at 121°C.

terpolymer (EPDM), and ethylene–propylene block copolymers (EP_bC) were used in the present work. The molecular characteristics, melt flow index (MFI), and other relevant information of these polymers is given in Table I.

Sample Preparation

Uniaxially drawn tapes of HDPE, PP, EP_bC, and various HDPE blends were prepared using a Betol-1820, single screw extruder, of L/D ratio 20, screw diameter of 18 mm, and a bottom fed slit die having width and thickness dimensions of 13 and 0.4 mm, respectively. The temperature profile for extrusion was 160°C at the feed zone, 200°C at the compression zone, and 220°C at the metering zone and the die end. The screw speed was kept at 12 rpm. The as-extruded tapes were immediately quenched in a water bath maintained at 30°C and were drawn in sequence on a 750-mm-long hot plate maintained at 95°C with a draw ratio of 10×. The drawn tapes were collected on a take-up bobbin with a speed of about 10 m/min. The drawn tapes were in the range of 950 and 1000 denier (denier is the weight in grams of 9000 meters of tape). The weight percent composition of blend components used for preparation of various blended tapes are summarized in Table II.

Characterization of Drawn Tapes

The drawn tapes were characterized for crystallite (f_c) and amorphous phase (f_{am}), orientation using combination of wide-angle X-ray diffraction (WAXD) and polarizing microscopy. Small-angle X-ray scattering (SAXS) was used to obtain the mean void dimensions in equatorial (l_e) and meridional (l_m), directions. The void number density per unit volume of tape (N_v) was obtained from total volume fraction of voids (ϕ_v) and the average volume of a void (V_e). The details of these characterization techniques, methods of analyses, assumptions made in the analysis of raw test data, extent of validity of the assumptions made, and the results have been discussed elsewhere.[32–34] The results of few selected specimens are given in Tables III and IV.

Fibrillation Analysis of Drawn Tapes Using Combined Tension–Twist Test

In this test a uniaxially oriented fibrillar tape of rectangular cross-section is twisted and then subjected

Table II Blend Composition for Various Blend Systems

Polymer Blend System	Blend Components	Blend Composition (wt %)
HDPE/ethylene copolymer blends	HDPE/HMWPE	90/10
	HDPE/LLDPE	90/10
	HDPE/LDPE	90/10
	HDPE/EVA	90/10
	HDPE/EPDM	90/10
HDPE/PP and HDPE/EP_bC blends	HDPE/PP or EP_bC	91/9
		82/18
		50/50
		20/80
		0/100

Table III Structural Characteristics of HDPE Tapes

Draw Ratio/ Drawing Temp. (°C)	$(1 - X_c)$	f_{am}	σ_f (MPa)	G_f (J)	l_e (Å)	l_m (Å)	$\phi_v \times 10^4$ (cm^3/cm^3)	$N_v \times 10^{-14}$ (cm^{-3})
3×/95	0.40	0.18	—	—	—	—	—	—
5×/95	0.40	0.34	—	—	150	91	3.8	5.8
7×/95	0.42	0.41	257	120	144	137	8.9	6.3
10×/95	0.26	0.50	220	86	122	144	15.6	13.9
14×/95	0.27	0.59	190	70	155	174	28.8	13.4
5×/120	0.37	0.23	—	—	—	—	5.9	—
10×/120	0.25	0.45	238	92	—	—	12.6	—
14×/120	0.23	0.60	202	77	112	147	11.7	12.1

to uniaxial loading as shown schematically in Fig. 1. Tape deforms elastically in a helical manner to some extent before local yielding begins. Then the stress state in the localized yield region of sample becomes triaxial,[35] which favors the initiation and growth of voids at weaker interfibrillar regions. The axial splitting (fibrillation) of tape occurs quite suddenly by accelerated growth and coalescence of voids in the orientation direction.

The following section describes the main characteristics of fibrous structure and stress distribution pattern, which forms the basis for our understanding of the microcrack formation, eventually leading to longitudinal splitting of tape in a combined tension–twist loading.

Fibrillar Morphology of Drawn Tapes

Drawing transforms the lamellar sample into a highly oriented fibrous structure with a completely new morphology.[1-5] The basic elements are microfibrils with an average length of ~ 10 μm and a diameter of ~ 100 Å. The microfibrils in the fibrous structure are highly aligned and bundled into fibrils (about 1000 Å wide) with small differences in local draw ratio, residual strain, and orientation of crystal lattice.[4] As a consequence, the lateral boundary of fibrils may be weaker than that of individual fibrils. Its weakness is further enhanced by the presence of the ends of microfibrils on the outer boundary of fibrils.[1-4] These point defects make the surface of the fibril less uniform and, thus, decrease the autoadhesion between adjacent fibrils. Hence, the boundary between fibrils permits axial shearing displacement and fails more easily than the boundary between microfibrils of the same fibril, thus yielding longitudinal voids so characteristic of highly drawn fibrous materials.[6-8,11]

Sze et al.[7] and Bodaghi et al.[6] have suggested a phenomenological explanation of the formation of voids in HDPE and PP, respectively. It is this problem and its interaction with structural and morphological parameters with which we are concerned in the present article. Generally, observations on fibrillation reported in the literature generally have been qualitative in character.[23-25]

Stress Distribution Pattern and Fibrillation of Tape in a Combined Tension–Twist Test

A oriented tape can be viewed as a body composed of uniaxially oriented fibrils that are held together by forces of cohesion. Initially the axes of fibrils are parallel to the tape axis [Fig. 2(a)]. In twisting, fibrils adopt a helical form [Fig. 2(b)]. Thus it follows that in every layer of fibrils of a twisted tape there must be present longitudinal and shear strains, the values of which are proportional to the distance of fibrils from the tape axis. If such a twisted tape is axially strained, complex stresses are generated.

A look at the microscopic twist and sample geometry will show that the center axis of the tape undergoes a compression, but on the edges of the tape, the situation is quite different. Here, fibrils are under a certain amount of tension and the shear force acting on these fibrillar elements is very high. Further straining of tape adds more shear stress to these fibrils, which finally leads to the initiation of vertical shear near the center of the tape, where a neutral plane is located [Fig. 2(c)]. Furthermore, with axial straining the reduction in overall diameter of twisted tape assembly induces a certain amount of bending forces on the edges of the tape, which act inwards, i.e., toward the center of twisted tape assembly [Fig. 2(e)]. The final splitting of the tape in the axial

Table IV Structural Characteristics of HDPE Blended Tapes

Sample	$(1 - X_c)$	f_{am} (avg)	σ_f (MPa)	G_f (J)	l_e (Å)	l_m (Å)	$\phi_v \times 10^4$ (cm^3/cm^3)	$N_v \times 10^{-14}$ (cm^{-3})
HDPE (control)	0.26	0.50	220	86	122	144	15.6	13.9
10 HMWPE	0.29	0.57	181	80	—	—	—	—
10 LLDPE	0.32	0.48	229	97	150	160	14.9	7.9
10 LDPE	0.33	0.43	247	103	163	169	21.5	9.2
10 EVA	0.40	0.39	275	128	151	156	17.1	9.2
10 EPDM	0.35	0.31	—	—	173	164	13.4	5.5
9 PP	0.30	0.50	208	88	158	173	18.3	8.1
18 PP	0.30	0.55	198	89	—	—	24.0	—
50 PP	0.41	0.30	—	—	169	190	25.8	9.1
80 PP	0.42	0.31	—	—	—	—	27.9	—
100 PP	0.35	0.44	196	76	154	161	22.2	11.2
9 EP_bC	0.39	0.49	245	127	148	159	15.0	8.2
18 EP_bC 1.5	0.30	0.51	228	131	—	—	16.1	—
50 EP_bC 1.5	0.43	0.47	151	81	—	—	14.5	—
80 EP_bC 1.5	0.44	—	—	—	—	—	19.3	—
100 EP_bC 1.5	0.45	0.42	242	116	—	—	14.3	—
9 EP_bC 3.5	0.39	0.53	237	123	163	172	18.9	7.9
18 EP_bC 3.5	0.37	0.53	244	105	—	—	19.8	—
50 EP_bC 3.5	0.41	0.32	—	—	174	191	28.7	9.5
80 EP_bC 3.5	0.41	0.34	189	76	—	—	30.2	—
100 EP_bC 3.5	0.44	0.42	236	121	160	178	23.6	9.9
9 EP_bC 7.0	0.31	0.37	231	97	—	—	19.8	—
50 EP_bC 7.0	0.54	0.34	176	72	—	—	36.1	—
9 EP_bC 13.0	0.25	0.41	238	80	165	188	21.9	8.2
18 EP_bC 13.0	0.23	0.53	196	72	—	—	35.5	—
50 EP_bC 13.0	0.41	0.36	175	66	—	—	—	—
80 EP_bC 13.0	0.42	0.36	169	61	—	—	47.0	—
100 EP_bC 13.0	0.43	0.48	211	111	152	171	30.5	14.7

direction, therefore, involves the opening of weaker interfibrillar regions at the center of the tape and subsequent axial shearing of fibrillar elements under the action of combined longitudinal, torsional, and bending forces [Fig. 2(d)].

In axial splitting of a tape, there are two important factors. One is the presence, distribution, and size of defects, such as elongated voids and microcracks at the interfibrillar region that strongly influence the nucleation and propagation of cracks.[3,6–8,11,23–26] The other is the inherent cohesiveness of fibrillar structure that opposes the separation of fibrillar elements.[3–5] The former effect is closely connected with gross morphology, whereas the latter with the interfibrillar molecular connections, the fraction of interfibrillar amorphous phase, its morphology, and its plastic deformation ability.

Testing Procedure and Equipment

The fibrillation behavior of oriented tapes was studied using an Instron tensile tester. The initial gauge length of a pretwisted tape specimen was maintained at 200 mm with a cross head speed of 100 mm/min. The uniaxially oriented tapes of about 2.2 mm width and 55–70 μm thickness were first gripped at the top jaw of the tensile tester and then were twisted to a predetermined twist angle (θ = 1080° and θ/l = 5.4°/mm) before clamping the other end of the tape at the bottom jaw. Extreme care was taken in mounting the tapes at the pneumatic grips. A slight deviation of sample axis from the longitudinal stress axis may generate undue shear forces in the sample.

The main variables recorded during the test were the angle of pretwist per unit length of tape and the corresponding longitudinal stress and longitudinal strain developed at the point of fibrillation. The

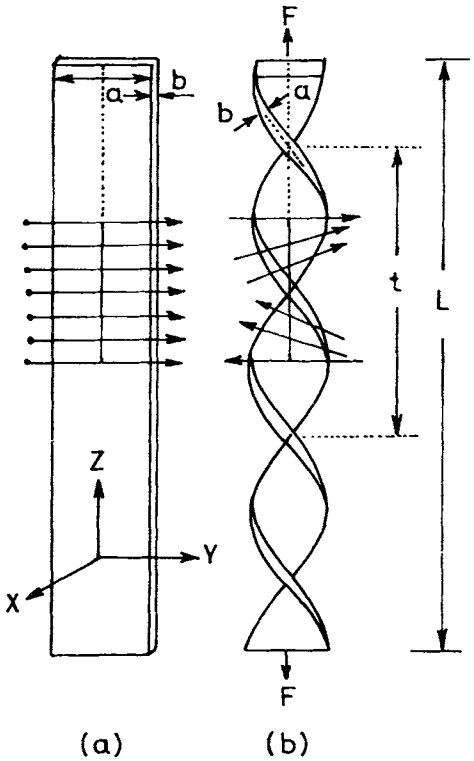

Figure 1 Tape arrangement during combined tension-twist test: flat tape (a); twisted tape during test (b). a, tape width; b, tape thickness; L, length of tape; t, twist period of 360°.

longitudinal stress required for axial splitting or fibrillation of a pretwisted tape (σ_f) is defined as the force (F) at fibrillation divided by the original cross-sectional area of tape. A typical load–extension curve is shown in Figure 3. The kink in the curve indicates the axial splitting of the tape during the test.

Test Analysis

Figure 4 shows the influence of pretwist per unit length (θ/l) on fibrillation strength (σ_f) and fibrillation strain (ϵ_f) determined by the combined tension–twist test. It is seen that the results are limited to the θ/l value ranging between 3.6 and 7.2. At θ/l less than 3.6, it was observed that the failure of the tape took place in a normal tensile mode, and no axial splitting was noticed. This effect may result from the insufficient level of pretwist imparted to the tape. The magnitude of shear stress generated as a result of pretwist is therefore very small and can be compensated for easily by the competitive process of the affine tilting of fibrils. Thus in this case the two competitive processes are balanced and hence the axial splitting of the tape becomes difficult.

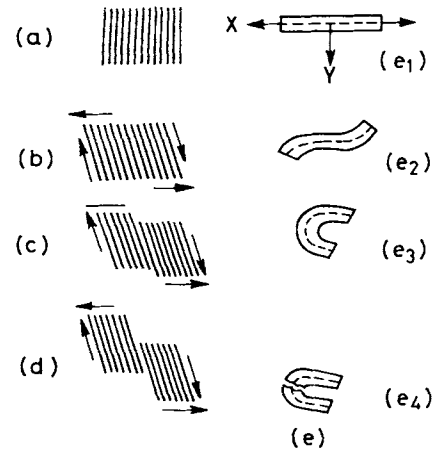

Figure 2 Schematic illustration of the step-wise fibrillation of tape during combined tension–twist test. (a) A finite element of tape illustrating fibril arrangement in a flat tape. (b) Fibril arrangement in a twisted tape. (c) Axial displacement of fibrillar elements. (d) Vertical shear and axial splitting of tape. (e) Cross section of tape corresponding to stages (a), (b), (c) and (d).

The gradual increase in level of pretwist beyond $\theta/l = 3.6$, however, systematically decreased the σ_f and ϵ_f. This effect appears to be the result of the combination of three main factors, viz., (i) a consistent increase in shear stress, (ii) bending of tape in x-y plane [Fig. 2(e)], and (iii) gradual opening of inerfibrillar amorphous regions.

At higher θ/l, the extent of shear stress generated as a result of pretwisting exceeds the rate of affine tilting of fibrils; hence, the shear stress becomes much more localized at interfibrillar amorphous regions. The final fibrillation in this case, therefore, occurs because of the concentration of finite shear

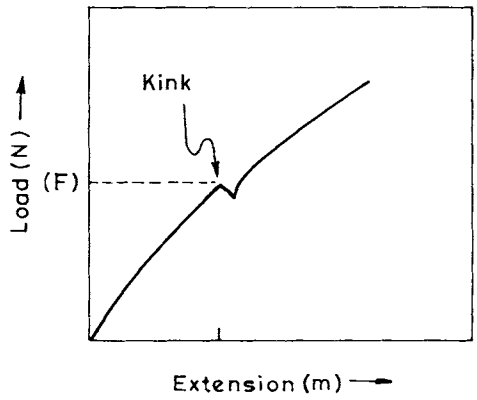

Figure 3 Typical load-extension curve of twisted tape during combined tension–twist test. The kink in the load-extension curve indicates the axial splitting of tape during the test.

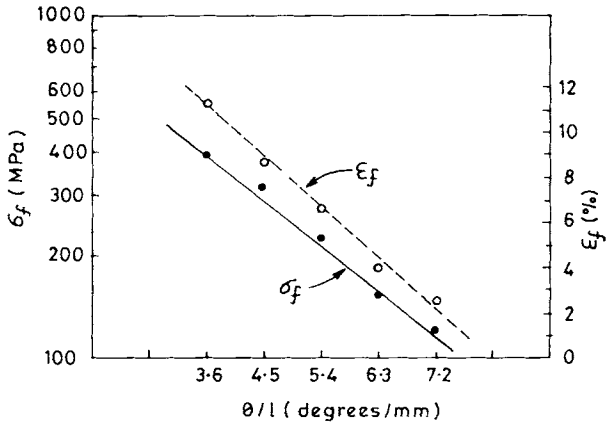

Figure 4 Effect of pretwist level on fibrillation strength and fibrillation strain of a drawn tape.

strains in the off-axially aligned interfibrillar narrow regions, leading to microvoid coalescence and localized verticle shearing process of fibrillar elements both at lower σ_f and ϵ_f.

RESULTS AND DISCUSSION

Effect of Amorphous Phase Orientation on Fibrillation Strength of Drawn Tapes

Figure 5 shows the relationship between fibrillation strength and amorphous phase orientation of drawn tapes. It is seen that the results are limited to a range of f_{am} between 0.4 and 0.6. At lower orientations, excessive plastic deformation accompanied with shape distortion of tape was observed, so that no meaningful measurements could be made. Specimens of fully developed fibrillar morphology with f_{am} greater than 0.4, however, showed a reasonably consistent fibrillation strength and fibrillation strain with a coefficient of variation between 3 and 7. From Figure 5, it is seen that fibrillation strength steadily decreases with increase in amorphous phase orientation. This is quite an expected result, because the increase in amorphous phase orientation achieved through post-neck deformation of fibrillar structure invariably yields weaker interfibrillar boundaries and axially elongated voids.[2-5] Because these regions transfer the applied stress less effectively in the transverse direction when loaded in a combined tension-twist mode, they act as elastic discontinuities in the structure. This increases the stress concentration at the preexisting microcracks. The data on void characteristics given in Tables III and IV clearly support this proposition. In general, it is seen that higher f_{am} is associated with the formation of axially elongated voids of larger dimensions. Furthermore, the volume fraction of voids and void number density increase accordingly.

In Figure 5, the noticeable deviation of fibrillation strength from the straight line relationship for 10 EVA, 9 EP_bC 1.5, 9 EP_bC 3.5, 18 EP_bC 3.5, and 50 EP_bC 1.5, 50 EP_bC 7.0, 50 EP_bC 13, 80 EP_bC 3.5, 80 EP_bC 13 blends is attributed to the differences in the morphology of interfibrillar amorphous regions.[32-34]

Previous investigations[32-34] of the morphology of these blends have revealed some important details of the gross phase morphology and interphase adhesion. The important morphological changes associated with the increase in composition of the second-blend component are as follows: (i) a systematic increase in phase segregation of blend components; (ii) a steady increase in crystallinity level; (iii) a drastic drop in tensile strength and elongation to break; and (iv) a significant increase in volume fraction of voids and average void dimensions both in equatorial and meridional directions (Table IV).

The changes in structural and morphological features of blends with an increase in blend composition are mainly the consequence of the gross incompatibility and phase segregation of blend components in HDPE/PP and HDPE/EP_bC blends. For these blends (50 and 80% blend composition), early yielding due to excessive stress concentration at weaker interphase boundaries and premature failure of in-

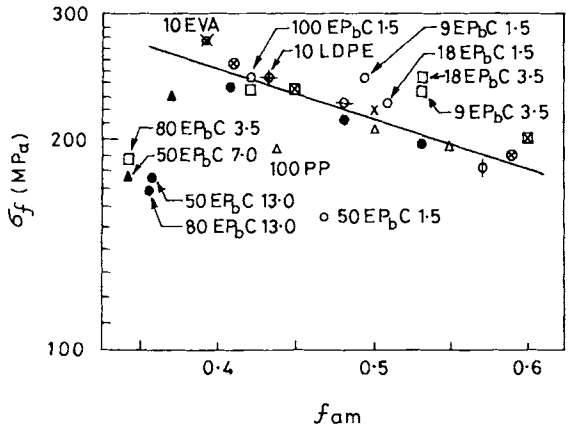

Figure 5 Fibrillation strength vs. amorphous phase orientation of HDPE and blended tapes. (×) HPDE (control); (⊗) HDPE (draw ratios 7×, 10×, 14×, drawing temperature 95°C; (⊠) HDPE (draw ratios 7×, 14×, drawing temperature 120°C); (ϕ) 10 HMWPE; (⊖) 10 LLDPE; (⊕) 10 LDPE; (⊠) 10 EVA; (+) 10 EPDM; (△) HDPE/PP; (○) HDPE/EP_bC 1.5; (□) HDPE/EP_bC 3.5; (▲) HDPE/EP_bC 7.0; (●) HDPE/EP_bC 13. For details refer to Tables III and IV.

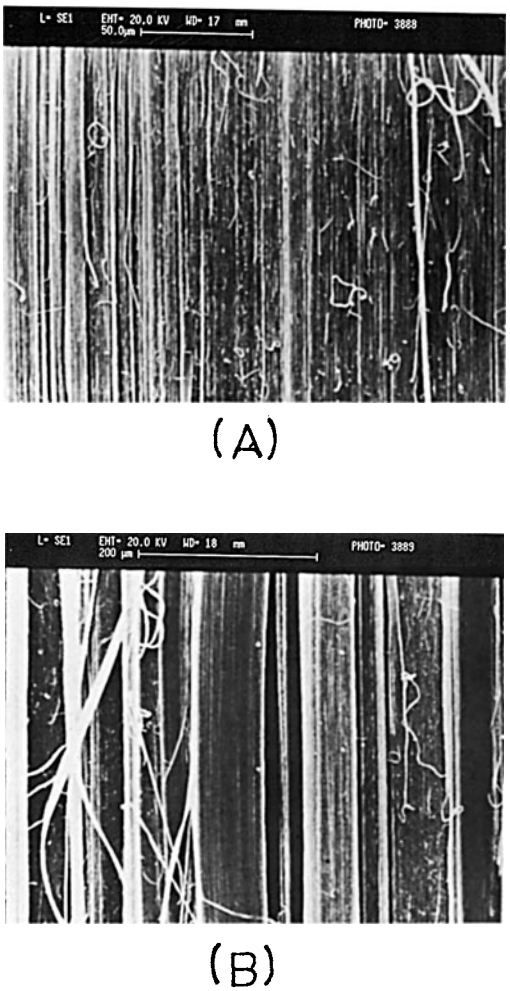

Figure 6 SEM micrographs of surface peeled drawn tapes. (A) HDPE and (B) 50 EP_bC 3.5 (draw ratio 10×, drawing temperature 95°C).

terphase may account for a sufficient degree of interfacial slippage to form longitudinal microcracks at large deformations. These morphological features are clearly seen in SEM micrographs of surface peeled drawn blended tapes shown in Figure 6.

For 10 EVA, 9 EP_bC 1.5, 9 EP_bC 3.5, 18 EP_bC 3.5, and 100 EP_bC 1.5 blends, the moderate increase in fibrillation strength, on the other hand, is related to the partial miscibility and higher degree of mutual interaction between the two blend components. During drawing, and particularly in the post–neck deformation stage, these specimens undergo homogeneous deformation and suppress the localized fibrillar slippage and formation of elongated voids, thus rendering the fibrillar structure less susceptible for formation of longitudinal microcracks at interfibrillar regions. As a consequence, these blended tapes have higher resistance to crack opening and propagation because of the reduction in the number of adventitious elliptical flaws at interfibrillar amorphous regions and also because of the homogeneous distribution of applied torsional stress caused by higher degree of interfibrillar connectivity and extensive molecular network.[32–34]

Effect of Amorphous Phase Orientation and Fraction of Amorphous Phase on Fibrillation Toughness of Drawn Tapes

Figure 7 shows the dependence of fibrillation toughness on amorphous phase orientation of drawn tapes. It is seen that the fibrillation toughness or energy required to fibrillate the tape steadily decreases with increase in amorphous phase orientation. This is related to the reduction in interfibrillar cohesion and formation of voids during the orientation process.

The dependence of fibrillation toughness on fraction of amorphous phase is shown in Figure 8. In spite of the relatively large scatter of results, there is a clear increase in fibrillation toughness with the increase in fraction of amorphous phase; hence, the data points follow a relatively linear relationship. These results may be interpreted in terms of the extent of plastic deformation occuring in the vicinity of growing crack tip, which in turn depend on the combination of the effects of amorphous fraction, interfibrillar connectivity, and amorphous phase orientation.

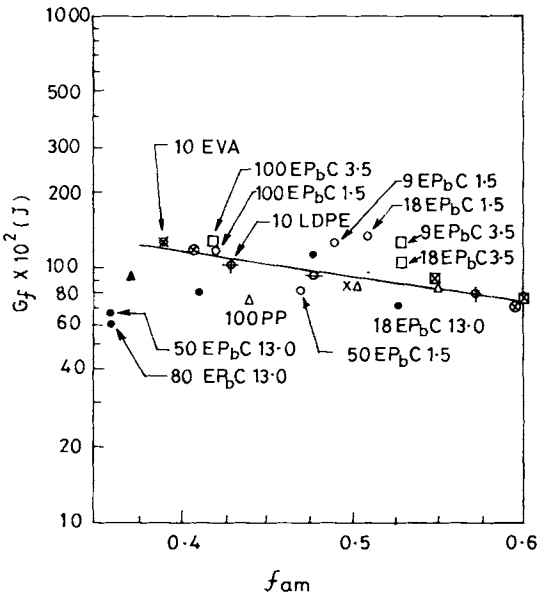

Figure 7 Fibrillation toughness vs. amorphous phase orientation for HDPE and blended tapes. Symbols as indicated in Fig. 5.

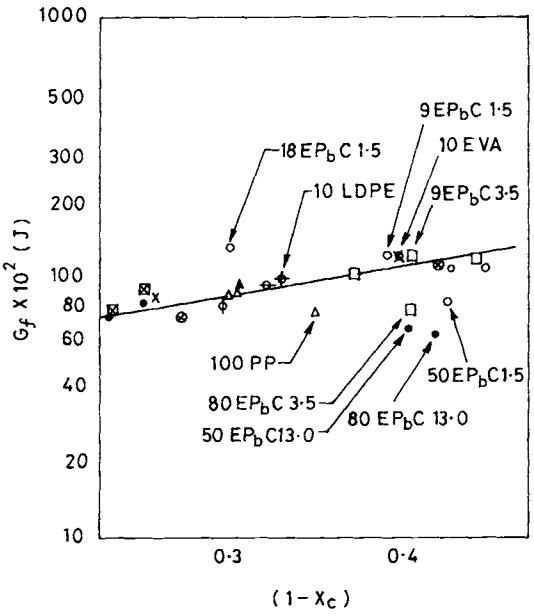

Figure 8 Fibrillation toughness vs. fraction of amorphous phase for HDPE and blended tapes. Symbols as indicated in Fig. 5.

For specimens containing a higher fraction of amorphous phase, a much greater volume of material is involved in the energy-dissipating plastic deformation processes during fibrillation. This multiple deformation mechanism results in relatively higher fibrillation strain and tough materials, although, the fibrillation strength of these tapes is comparable with other specimens.

In the above case, the extent of plastic deformation depends on molecular network and interfibrillar connectivity. If the fraction of interfibrillar tie molecules in the direction of applied shear stress is small, as is the case in highly oriented tapes, the microcracks will form at a lower shear stress and the crack propagation will predominate over the plastic deformation process. Any increase in the fraction of tie molecules in the direction of applied shear stress makes the separation of fibrillar elements more difficult and decreases the crack propagation rate.

As we have noted earlier, there are two features of the results for blends containing about 10% second-blend components, which are worthy of special interest: (a) the higher fraction of amorphous phase and concurrent with this higher values of toughness and (b) the predominant fibrillar fracture surface morphology compared with the blends of higher blend composition.

The possible causes of fibrillar fracture in drawn tapes may be related to the presence of crossover fibrillar ligaments as shown in SEM micrographs in Figures 9 and 10, and the interfibrillar tie molecules having wider contour length distribution. On crack propagation, these tie elements get strain hardened and eventually are pulled out of the matrix, depending upon their contour lengths, resulting in the observed fibrillar fracture surfaces as shown in Figure 11.

In partially miscible and compatible blends, such as 10 EVA, 9 EP_bC 1.5, 9 EP_bC 3.5, 18 EP_bC 1.5, 18 EP_bC 3.5, and 100 EP_bC 1.5 the molecular network is presumably more highly developed. Moreover, these blends also show a distinctly higher fraction of amorphous phase. These effects may arise because of a change in crystallization mechanism of HDPE component in the presence of poorly crystallizable copolymer molecules and the subsequent alteration

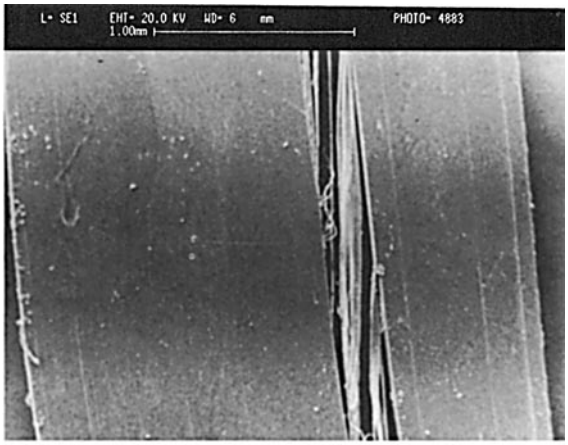

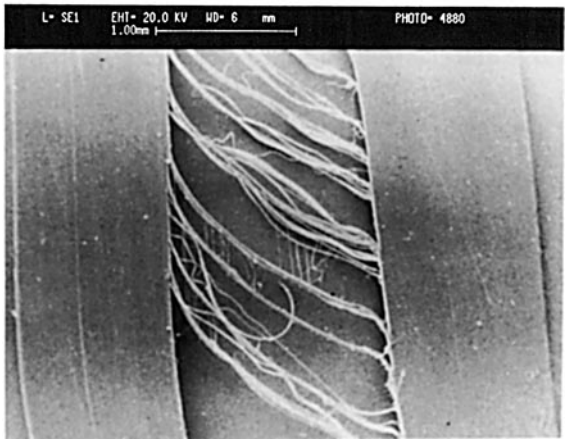

Figure 9 Typical SEM micrographs of the fibrillated portion of tape showing interconnected fibrillar network (draw ratio 10×, drawing temperature 95°C).

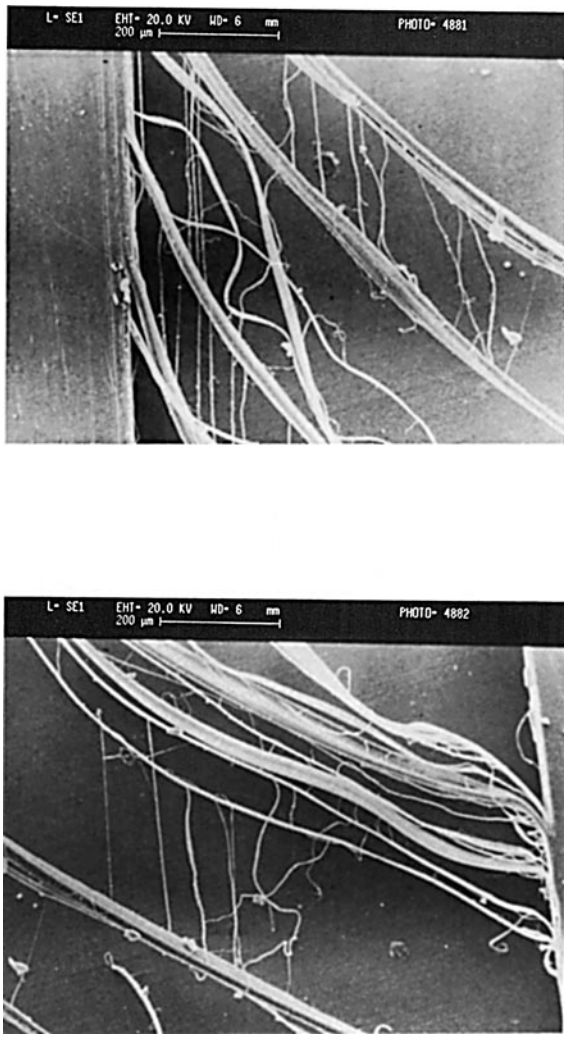

Figure 10 SEM micrographs of crack shown in Fig. 9 at higher magnification.

in the molecular topology of the amorphous phase.[32,33] Thus, in this case, because of the highly developed molecular network and a higher fraction of amorphous phase, the molecular pull-out becomes more difficult and fibrillation occurs after extensive plastic yielding and at larger strains, leading to higher fibrillation toughness than immiscible, phase segregated blends.

CONCLUSIONS

From the limited experimental data presented here, it is seen that the fibrillation strength of drawn tapes decreases linearly with amorphous phase orientation. This is attributed to the reduction in number of interfibrillar tie molecules in the lateral direction, formation of elongated voids, and excessive stress concentration at the crack tip.

The effect of polymer blending on fibrillation strength of HDPE is rather complex. At low blend compositions (<20%), the fibrillation strength is increased by 15–30% over the control specimen. In contrast, at higher blend compositions, the fibrillation strength is decreased by almost 40%. This latter effect is related to the following:

1. immiscibility and poor interphase adhesion.
2. formation of elongated voids and microcracks of larger dimensions, and
3. poor interfibrillar cohesion and mechanical connectivity.

The best prospects for production of drawn tapes of polyethylene with reasonably low fibrillation tendency are obtained by blending up to 10% ethylene copolymers to linear polyethylene. This is achieved through formation of dense molecular network and improved interfibrillar connectivity.

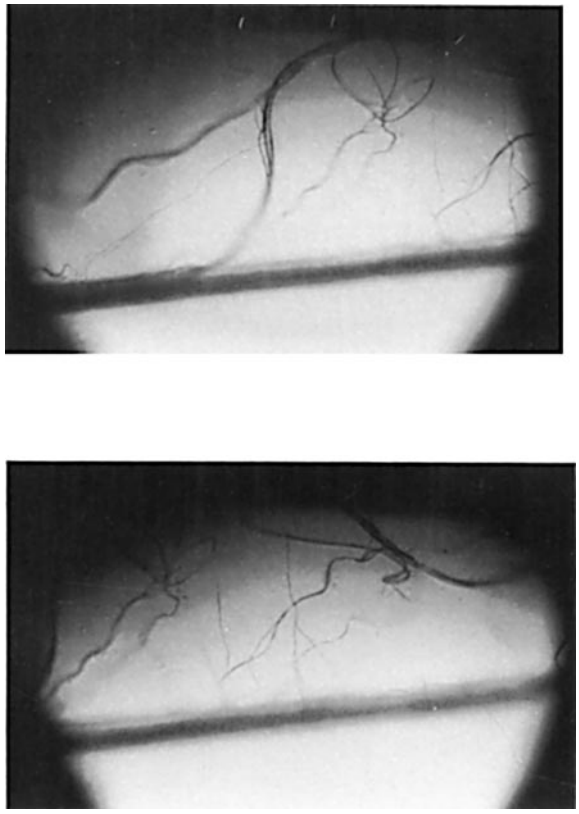

Figure 11 Typical micrograph of the fracture surface of fibrillated tape showing pulled out fibrillar elements (draw ratio 10×, drawing temperature 95°C).

REFERENCES

1. A. Peterlin, *Textile Res. J.*, **42,** 20 (1972).
2. A. Peterlin, *Polym. Eng. Sci.*, **17,** 183 (1977).
3. A. Peterlin, *Intern. J. Fracture,* **11,** 761 (1975).
4. A. Peterlin, in *Ultrahigh Modulus Polymers,* A. Cifferi and I. M. Ward, Eds., Applied Science Publishers, London, 1977, p. 279.
5. A. Garton, D. J. Carlsson, P. Z. Sturgeon, and D. M. Wiles, *J. Polym. Sci., Polym. Phys. Ed.*, **15,** 2013 (1977).
6. H. Bodaghi, J. E. Spruiell, and J. L. White, *Intern. Polymer Processing,* **III** (2), 100 (1988).
7. G. M. Sze, J. E. Spruiell, and J. L. White, *J. Appl. Polym. Sci.*, **20,** 1823 (1976).
8. L. F. Min, B. C. Goswami, J. E. Spruiell, and K. E. Duckett, *J. Appl. Polym. Sci.*, **30,** 1859 (1985).
9. K. E. Duckett and B. C. Goswami, *Textile Res. J.*, **54,** 43 (1984).
10. B. C. Goswami, K. E. Duckett, and T. L. Vigo, *Textile Res. J.*, **50,** 481 (1980).
11. K. L. Devries, R. D. Luntz, and M. L. Williams, *J. Polym. Sci., Polym. Lett. Ed.*, **10,** 409 (1972).
12. I. Tsujimoto, T. Kurokawa, T. Takahashi, and K. Sakurai, *J. Appl. Polym. Sci.*, **24,** 2289 (1979).
13. I. Tsujimoto, T. Kurokawa, T. Takahashi, and K. Sakurai, *J. Appl. Polym. Sci.*, **24,** 2303 (1979).
14. M. Kurukawa, N. Nohara, and T. Konishi, *J. Appl. Polym. Sci.*, **26,** 1613 (1980).
15. N. V. Hien, S. L. Cooper, and J. A. Koutsky, *J. Macromol. Sci., Phys. Ed.*, **B6,** 343 (1972).
16. S. J. Deteresa, S. R. Allen, R. J. Farris, and R. S. Porter, *J. Mater. Sci.*, **19,** 57 (1984).
17. R. Greer and J. W. S. Hearle, *Polymer,* **11,** 441 (1970).
18. S. F. Calil, I. E. Clark, and J. W. S. Hearle, *J. Mater. Sci.*, **24,** 736 (1989).
19. M. Toney and P. Schwartz, *J. Appl. Polym. Sci.*, **46,** 2023 (1992).
20. J. Grebowicz, T. Pakula, M. Kryszewski, and Z. Pelzbauer, *Polymer,* **20,** 1281 (1979).
21. C. Y. C. Lee and U. Santhosh, *Polym. Eng. Sci.*, **33,** 907 (1993).
22. W. F. Knoff, *J. Mater. Sci., Lett. Ed.*, **6,** 1392 (1987).
23. J. Baldarin, in *Morphology of Polymers,* Blahoslav Sedlacek, Ed., Walter de Gruyter, Berlin, New York, 1986, p. 661.
24. G. J. Sandilands and J. R. White, *J. Mater. Sci., Lett. Ed.*, **12,** 1496 (1977).
25. P. Robson, G. J. Sandilands, and J. R. White, *J. Appl. Polym. Sci.*, **26,** 3515 (1981).
26. N. H. Ladizesky and I. M. Ward, *J. Mater. Sci.*, **23,** 72 (1988).
27. M. M. Sadowski, T. H. North, and G. C. Weatherly, *J. Mater. Sci., Lett. Ed.*, **10,** 1007 (1991).
28. K. Sukai and N. Nishikawa, *Kobunshi Ronbunshu,* **44**(7), 515 (1987).
29. L. A. Martynova, V. I. Selikhova, Y. A. Zubor, and M. P. Zverev, *Fibre Chem.*, **12,** 12 (1980).
30. L. A. Polovikhina, I. G. Shimko, and M. P. Zverev, *Fibre Chem.*, **10,** 13 (1978).
31. L. A. Martynova, M. P. Zverev, and V. A. Isenko, *Fibre Chem.*, **11,** 23 (1979).
32. S. J. Mahajan, B. L. Deopura, and Yimin Wang, *J. Appl. Polym. Sci.* **00,** 0000 (1996).
33. S. J. Mahajan, B. L. Deopura, and Yimin Wang, *J. Appl. Polym. Sci.*, **00,** 0000 (1996).
34. S. J. Mahajan, B. L. Deopura, and Yimin Wang, *J. Appl. Polym. Sci.*, **00,** 0000 (1996).
35. E. H. Andrews, *Developments in Polymer Fracture—I,* Applied Science Publishers Ltd., London, 1979.

Received June 16, 1994
Accepted October 7, 1995